Peridynamics analysis of the nanoscale friction and wear properties of amorphous carbon thin films

S. Ebrahimi, **D. Steigmann** and **K. Komvopoulos**[1]

Department of Mechanical Engineering
University of California
Berkeley, CA 94720, USA

Abstract

Peridynamics theory was used to study the nanoscale friction and wear processes of thin films of amorphous carbon used as protective overcoats in hard-disk drives. The length scale parameter (horizon) used in state-based peridynamics theory was used to account for the multi-scale physical processes examined in this study. Analytical results of the coefficient of friction and wear depth are shown to be in good agreement with published experimental results. Although long-range forces are not considered in the analysis, the results indicate that the present approach yields fairly accurate estimates of the coefficient of friction and wear depth for a film thickness greater than 10 nm and a grid size of 1.78 nm. The results of this study demonstrate that peridynamics theory can be used to analyze various nanoscale friction and wear phenomena without being limited by the excessive computational time and convergence problems encountered with traditional numerical methods.

1. Introduction

Carbon thin films are used as protective overcoats in a wide range of applications where the tribological properties of proximal surfaces are of paramount importance to the functionality and endurance of mechanical components possessing contact interfaces. For example, thin films of amorphous carbon (a-C) play a critical role in the reliability and performance of magnetic recording devices because they protect the head and hard disk surfaces against mechanical wear during intermittent surface contact and inhibit corrosion of the magnetic medium in the hard disk. In view of the extremely small thickness of a-C films and occurrence of head-disk surface interaction at nanoscopic surface protrusions (asperities), knowledge of the nanoscale tribological and mechanical properties of a-C thin films is of high technological importance.

The nanoscale mechanical and tribological properties of a-C films are greatly affected by carbon atom hybridization and hydrogen content. Other elements, such as Si, N, B, F, and O, may be added to modify the electromechanical properties of a-C films [1]. The structure and elemental content of a-C films strongly depend on the intricacies of the deposition process that controls film nucleation and growth [1–3]. Thus, small variations in the deposition conditions may result in vastly different film properties. Because of time consuming experimental techniques for nanomechanical/tribological testing of very thin films, alternative approaches must be used to identify the effects of structural changes on the resulting film properties.

High contents of tetrahedral carbon atom hybridization (sp^3) characterize the structure of a-C films exhibiting diamond-like behavior, whereas high contents of trigonal carbon atom hybridization (sp^2) generally produce graphitic-like film behavior. Continuum matter description does not account for local nanostructure differences [4], whereas molecular dynamics (MD) analyses are limited by high computational cost, small model size, and potential function used to model atom-atom

[1]Corresponding author (E-mail:kyriakos@me.berkeley.edu, Tel.: (510) 642-2563, Fax: (510) 642-5539)

interactions [5]. Therefore, nonlocal computational approaches that are not subjected to the aforementioned restrictions must be developed to more effectively study the interdependence of structure and material behavior at the nanoscale.

Peridynamics [6] is a fairly new computational approach that promises to bridge this gap in computational mechanics of materials. Peridynamics is a continuum version of MD which uses integral equations of motion to offset complexities in modeling material discontinuities (e.g., defects, edges, and sharp corners) instead of conventional partial differential equations used in classical mechanics and does not rely on an a priori assumed damage criterion (e.g., crack growth direction). Because of the mathematical simplicity and computational affordability of peridynamics, it has been used to analyze various computationally intense problems, such as dynamic fracture in brittle [7–11] or composite [12–16] materials, multi-scale damage [17, 18], and damage of nanofiber networks including long-range effects of van der Waals forces on nanofiber deformation [19–22]. Peridynamics has also been used in failure analyses dealing with thin-film cracking in electronic packaging [23–25] and, in conjunction with atomic force microscopy/nanoindentation, to determine the mechanical properties of ultrathin films [26].

The objective of this study is to introduce a two-dimensional (2D) peridynamics analysis of the nanotribological behavior of thin a-C films. Simulation results of the coefficient of friction and wear depth due to a diamond tip sliding against a-C films of different thickness and nanomechanical properties are presented and compared with similar experimental results of a previous study [27] to validate the accuracy of the developed peridynamics models.

2. State-based peridynamics formulation

Peridynamics is a numerical method that uses a finite number of particles to model a deformable body. Particle interaction is modeled within a predefined distance, referred to as the horizon. The governing equations in peridynamics are in integral form of particle motion, facilitating the modeling of material discontinuities and high strain gradients. The main peridynamics approaches can be classified as bond-based and state-based formulations. Bond-based peridynamics presume the existence of a pair-wise force function between any two particles, which is independent of the deformation of other particles [6] and has been developed for a Poisson's ratio of 0.33 and 0.25 for (2D) and three-dimensional (3D) problems, respectively. State-based peridynamics is based on a more general theory that uses a more comprehensive constitutive model derived from force- and deformation-state concepts [28]. To obtain the force state at each particle, the deformation of all the bonds within the particle's horizon are considered without invoking a specific Poisson's ratio value. Similarities between state-based peridynamics and continuum theory have been reported [28, 29], including the convergence of state-based peridynamics to classical elasticity theory [30].

The general 3D peridynamics equation is given by [28]

$$\rho(\mathbf{x}_i)\ddot{\mathbf{u}}(\mathbf{x}_i,t) = \int_{\mathcal{H}} \Big(\underline{\mathbf{T}}[\mathbf{x}_i,t]\langle \mathbf{x}_j - \mathbf{x}_i\rangle - \underline{\mathbf{T}}[\mathbf{x}_j,t]\langle \mathbf{x}_i - \mathbf{x}_j\rangle\Big)\mathrm{d}V_j + \mathbf{b}(\mathbf{x}_i,t) \tag{1}$$

where ρ is the mass density, $\mathbf{u}$ is the displacement field, $\mathcal{H}$ is the domain of the spherical horizon with a radius δ, $\underline{\mathbf{T}}$ is the force vector state field, $\mathbf{b}$ is the body force density field, t is the time, and $\mathrm{d}V_j$ is the j^{th} particle's volume. In the present analysis, all the materials are considered to be ordinary, implying the force between two particles acts along their bond.

For ordinary materials, the force vector is given by [28]

$$\underline{\mathbf{T}} = \underline{t}\underline{\mathbf{M}} \tag{2}$$

where $\underline{t}$ is the scalar force state and $\underline{\mathbf{M}}$ is the deformation direction vector. In the linear peridynamics solid (LPS) model, the force scalar state is defined by [28]

$$\underline{t} = \frac{3K\theta[\mathbf{x},t]}{m[\mathbf{x}]}\underline{\omega}\langle\boldsymbol{\xi}\rangle\,\underline{x}\langle\boldsymbol{\xi}\rangle + \frac{15G}{m[\mathbf{x}]}\underline{\omega}\langle\boldsymbol{\xi}\rangle\,\underline{e}^{\mathrm{d}}[\mathbf{x},t] \tag{3}$$

where K and G are the bulk and shear modulus, respectively, θ is the dilatation, m is the weighted volume, $\underline{e}^d$ is the deviatoric component of the extension scalar state $\underline{e}$, and $\underline{\omega}$ is the influence function. These parameters can be defined as following [28]:

$$\theta[\mathbf{x},t] = \frac{3}{m[\mathbf{x}]}\int_{\mathcal{H}}\underline{\omega}\langle\boldsymbol{\xi}\rangle\,\underline{x}\langle\boldsymbol{\xi}\rangle\,\underline{e}[\mathbf{x},t]\langle\boldsymbol{\xi}\rangle\mathrm{d}V \tag{4}$$

$$m[\mathbf{x}] = \int_{\mathcal{H}}\underline{\omega}\langle\boldsymbol{\xi}\rangle\,\underline{x}\langle\boldsymbol{\xi}\rangle\,\underline{x}\langle\boldsymbol{\xi}\rangle\,\mathrm{d}V \tag{5}$$

$$\underline{e}[\mathbf{x},t]\langle\boldsymbol{\xi}\rangle = \|\boldsymbol{\xi}+\boldsymbol{\eta}\| - \|\boldsymbol{\xi}\| \tag{6}$$

$$\underline{e}^d[\mathbf{x},t]\langle\boldsymbol{\xi}\rangle = \underline{e}[\mathbf{x},t]\langle\boldsymbol{\xi}\rangle - \underline{e}^i[\mathbf{x},t]\langle\boldsymbol{\xi}\rangle = \underline{e}[\mathbf{x},t]\langle\boldsymbol{\xi}\rangle - \frac{1}{3}\theta[\mathbf{x},t]\,\underline{x}\langle\boldsymbol{\xi}\rangle \tag{7}$$

where $\boldsymbol{\xi} = \mathbf{x}_j - \mathbf{x}_i$ is the relative position vector between two particles i and j in the reference configuration and $\boldsymbol{\eta} = \mathbf{u}(\mathbf{x}_j,t) - \mathbf{u}(\mathbf{x}_i,t)$ is the relative displacement vector between particles i and j at time t.

Because of the highly disordered structure of a-C films [1], they can be modeled as isotropic materials with an influence function $\underline{\omega}\langle\boldsymbol{\xi}\rangle = 1/\|\boldsymbol{\xi}\|$, as suggested elsewhere [31].

Damage is assumed to occur when bond stretching exceeds a predefined critical stretch s_c given by [7, 32]

$$s_c = \sqrt{\frac{4\pi G_I}{9E\delta}} \tag{8}$$

where G_I is the critical energy release rate corresponding to the mode I stress intensity factor K_I (*i.e.*, $G_I = K_I^2/E'$, where $E' = E$ (plane stress) or $E/(1-\nu^2)$ (plane strain)). Eq. (8) indicates that s_c is a function of the material properties and the characteristic length scale of the analyzed body (*i.e.*, horizon radius δ).

3. Body discretization and computational details

To obtain a 2D solution of Eq. (1), the body is discretized by a uniform grid ($\Delta x = \Delta y$) and the integral is replaced by a summation that includes all interacting particles within the horizon of a given particle. Thus, Eq. (1) can be expressed as

$$\rho_i\,\ddot{\mathbf{u}}_i^n = \sum_{j=1}^{N_{\mathcal{H}}}\mathcal{F}\big(\mathbf{x}_i^n,\mathbf{x}_j^n,\mathbf{x}_i^{n-1},\mathbf{x}_j^{n-1}\big)(\Delta x)^2 + \mathbf{b}_i^n \tag{9}$$

where the superscripts denote the time step. Time integration of Eq. (9) using the velocity-Verlet algorithm [33] yields the location and velocity of each particle at time step $(n+1)$. Because this is a 2D formulation, the nodal volume is replaced by the nodal area $(\Delta x)^2$; however, the nodal area of particles laying at horizon boundaries is accordingly modified.

In addition to the force vector state obtained from Eq. (2), short-range forces are also included in the present analysis by using a short-range interaction radius $d_{pi} = \min\{0.9\,\|\mathbf{x}_p - \mathbf{x}_i\|, 1.35(r_p + r_i)\}$,

where r_i is the radius of the i^{th} particle and is chosen to be equal to one-half of the grid size (*i.e.*, $r_i = \Delta x/2$). Long-range forces may also have a strong effect on nanoscale deformation and, despite the continuum nature of peridynamics, it is possible to incorporate potential force functions from MD analysis in the force state of peridynamics [19, 21, 22]. However, for a separation distance of 2 nm, long-range forces reach ∼10% of their peak values [19]. Hence, since the grid size used in the present analysis is less than 2 nm (see section 4 for details), long-range forces are not considered for simplicity.

4. Peridynamics friction and wear models

State-based peridynamics friction and wear models are presented in this section and simulation results are compared with experimental data of a previous study of the nanoscale tribological properties of thin a-C films [27] to illustrate the validity of the developed models. All simulations were carried out with a custom-made peridynamics code written in Fortran 90/95 and executed on a Linux platform with a quad-core 2.33 GHz Intel Xeon E5345 CPU.

4.1. Friction model

Fig. 1 schematically shows a diamond probe with a spherical tip of radius $R = 20$ μm sliding against a thin a-C film supported by a thick Si substrate. The elastic properties and density of the Si substrate and diamond tip are given in Table 1 whereas the film thickness, root-mean-square (rms) surface roughness, elastic properties, and density are given in Table 2. The critical stretch for the stronger a-C/diamond interface and the weaker a-C/Si interface is assumed to be equal to 0.03 and 0.007, respectively. The film density was calculated from the relation $\rho = 1.37 + E^{2/3}/44.65$, where ρ and E are expressed in g/cm^3 and GPa, respectively [34]. All materials are assumed to be isotropic, predominantly exhibiting brittle behavior. In all simulations, the sliding speed and total distance of sliding are fixed at 0.4 μm/s and 4 μm, respectively, whereas the normal load is varied in the range of 50-400 μN, similar to the experimental conditions of the nanoscale friction and wear study of Lu and Komvopoulos [27]. A thin layer at the bottom of the substrate and the top of the probe tip is modeled as rigid. The low Poisson's ratio of diamond ($\nu = 0.07$) precludes the use of bond-based peridynamics, whereas the dominance of elastic deformation under the above testing conditions [27] allows LPS modeling. Moreover, a-C films of thickness greater than 10 nm are examined because the grid size is <2 nm. In addition, because the rms surface roughness of the films (in the range 0.15–0.51 nm [27]) is significantly smaller than the grid size, the film and substrate media are modeled as ideally flat. Based on the stability condition proposed in a previous study [32], a time step of 0.1 ps (depending on the material properties and horizon radius) should suffice in all simulations. However, the estimated time step was multiplied by 0.1 to account for any possible nonlinearity effects in the simulations [35].

4.2. Wear model

Fig. 2 shows a schematic of the wear model involving a sharp ($R = 100$ nm) diamond tip sliding and plowing through an a-C film on a 1 μm × 1 μm Si substrate. The depth of the wear mark produced onto the film surface by the diamond tip under a normal load of 10 μN and constant sliding speed (4 μm/s) is used to quantify the film wear resistance. The thickness, rms roughness, and elastic properties, and density of the a-C films analyzed by the peridynamics wear model are given in Table 3.

5. Results and discussion

Simulation results obtained with the peridynamics friction and wear models are presented in this section in conjunction with experimental results of a previous study [27] for the same test conditions.

5.1. Coefficient of friction

The coefficient of friction is defined as the ratio of the tangential (friction) force and the applied normal load. Similar to local numerical methods, determining an appropriate grid size in peridynamics requires convergence testing [8, 36]. Among various convergence tests, the m-convergence test was applied to the peridynamics friction model to calculate the coefficient of friction. The $\delta-$convergence test was not used in this study because the decrease of the horizon to zero (*i.e.*, no length scale) should yield solutions converging to classical elasticity solutions, which not only do not hold at the nanoscale [4] but are also length-scale independent. In the $m-$convergence test, δ is fixed whereas $m = \delta/\Delta$x is gradually increased until the solution convergences to an exact nonlocal peridynamics solution obtained for a fixed δ [36]. Table 4 shows results from $m-$convergence tests of film #7 (Table 2) for a normal load of 100 μN, $\delta = 8$ nm, and m varied between 3.0 and 5.0. The coefficient of friction diverges with the increase of m from 4.5 to 5.0, suggesting an increasing effect of long-range forces. Therefore, $m = 4.5$ (*i.e.*, $\Delta x = 1.78$ nm) was used in the present peridynamics analysis. Because the focus of this study is the analysis of thin a-C films, $m = 3.0$ was selected for both the diamond tip and the Si substrate with $\Delta x = 1$ μm and 2 nm, respectively as $m = 3.0$ has been generally proven to be a reasonable choice for the horizon [32].

Table 5 shows a comparison between numerical and experimental coefficients of friction of a-C films of different thickness and rms surface roughness in the 50-400 μN load range. Despite the fact that both the film and the tip were modeled to have ideally smooth surfaces, the agreement between analytical and experimental results is good. It is noted that the experimental coefficients of friction are calculated as averages of 300 data obtained along the entire sliding track and that scatter in the measurements increases with decreasing load, yielding standard deviation values in the range of 0.05–0.08 [27]. In contrast to the experimental data, peridynamics friction analysis yields a uniform coefficient of friction response without errors due to data scatter or averaging effects.

Fig. 3 shows a comparison between analytical and experimental results of a typical coefficient of friction response for a 400 μN normal load. The analytical solution closely follows the experimental trend, showing a good agreement with the average response of the scattered experimental data. Fig. 3 and Table 6 illustrate the validity of the peridynamics friction model and provide justification for the modeling assumptions.

Fig. 4 shows analytical results of the steady-state coefficient of friction (obtained as the average of numerical data over the 0 to 4 μm sliding distance range from versus normal load for four different a-C films (Table 2). All solutions show that the coefficient of friction decreases with increasing normal load. This trend is in good agreement with experimental findings, and is attributed to the inverse proportionality of the coefficient of friction of predominantly elastically deformed surfaces to the cubic root of the normal load [27].

5.2. Wear depth

To validate the peridynamics wear model, the experimentally measured depth of the wear track produced on a-C films by a sharp diamond tip [27] was compared with analytical results. The wear

depth is defined as the maximum plowing depth averaged over the entire wear track. Table 6 shows analytical and experimental results of the wear depth for three a-C films and normal load equal to 10 μN. For films #8 and #9 the agreement is good ($\sim$ 5% error), while the agreement for film #10 is fair, presumably because of the higher roughness of this film and errors due to the small film thickness (10 nm) relative to the grid size (1.78 nm).

6. Conclusions

Nanoscale material behavior can be challenging because classical continuum theory breaks down while MD analysis is limited to smaller scales. Peridynamics promises to bridge this gap in computational mechanics of materials. In this study, state-based peridynamics theory was used to develop friction and wear models of thin films. Favorable comparisons between peridynamics solutions and experimental results of a-C thin films obtained under identical test conditions illustrated the validity of the peridynamics friction and wear models. Long-range forces were not considered in the present analysis and the film surfaces were modelled as ideally smooth because the film surface roughness was significantly smaller than the grid size. Despite these assumptions, a good agreement was observed between peridynamics and experimental results for film thickness greater than 10 nm. The results of this study demonstrate the potential of peridynamics to capture the nanoscale tribological behavior of thin films, which is difficult (if not impossible) to achieve with other numerical techniques at the nanoscale, such as the finite element method.

Acknowledgments

This research was partially funded by the Computer Mechanics Laboratory, University of California, Berkeley.

References

[1] C. Charitidis, "Nanomechanical and nanotribological properties of carbon-based thin films: a review," *International Journal of Refractory Metals and Hard Materials*, vol. 28, no. 1, pp. 51–70, 2010.

[2] Y. Lifshitz, "Hydrogen-free amorphous carbon films: correlation between growth conditions and properties," *Diamond and Related Materials*, vol. 5, no. 3, pp. 388–400, 1996.

[3] A. Grill, "Diamond-like carbon: state of the art," *Diamond and related materials*, vol. 8, no. 2, pp. 428–434, 1999.

[4] B. Luan and M. O. Robbins, "The breakdown of continuum models for mechanical contacts," *Nature*, vol. 435, no. 7044, pp. 929–932, 2005.

[5] B. J. Alder and T. Wainwright, "Studies in molecular dynamics. I. general method," *Journal of Chemical Physics*, vol. 31, no. 2, pp. 459–466, 1959.

[6] S. A. Silling, "Reformulation of elasticity theory for discontinuities and long-range forces," *Journal of the Mechanics and Physics of Solids*, vol. 48, no. 1, pp. 175–209, 2000.

[7] Y. D. Ha and F. Bobaru, "Characteristics of dynamic brittle fracture captured with peridynamics," *Engineering Fracture Mechanics*, vol. 78, no. 6, pp. 1156–1168, 2011.

[8] F. Bobaru and W. Hu, "The meaning, selection, and use of the peridynamic horizon and its relation to crack branching in brittle materials," *International journal of fracture*, vol. 176, no. 2, pp. 215–222, 2012.

[9] W. Liu and J.-W. Hong, "Discretized peridynamics for brittle and ductile solids," *International Journal for Numerical Methods in Engineering*, vol. 89, no. 8, pp. 1028–1046, 2012.

[10] R. Lipton, "Dynamic brittle fracture as a small horizon limit of peridynamics," *Journal of Elasticity*, pp. 1–30, 2014.

[11] Y. D. Ha and F. Bobaru, "Studies of dynamic crack propagation and crack branching with peridynamics," *International Journal of Fracture*, vol. 162, no. 1-2, pp. 229–244, 2010.

[12] E. Askari, J. Xu, and S. Silling, "Peridynamic analysis of damage and failure in composites," in *44th AIAA Aerospace Sciences Meeting and Exhibit, Reno, NV: AIAA*, 2006.

[13] J. Xu, A. Askari, O. Weckner, and S. Silling, "Peridynamic analysis of impact damage in composite laminates," *Journal of Aerospace Engineering*, vol. 21, no. 3, pp. 187–194, 2008.

[14] B. Kilic, A. Agwai, and E. Madenci, "Peridynamic theory for progressive damage prediction in center-cracked composite laminates," *Composite Structures*, vol. 90, no. 2, pp. 141–151, 2009.

[15] W. Hu, Y. D. Ha, and F. Bobaru, "Modeling dynamic fracture and damage in a fiber-reinforced composite lamina with peridynamics," *International Journal for Multiscale Computational Engineering*, vol. 9, no. 6, 2011.

[16] W. Hu, Y. D. Ha, and F. Bobaru, "Peridynamic model for dynamic fracture in unidirectional fiber-reinforced composites," *Computer Methods in Applied Mechanics and Engineering*, vol. 217, pp. 247–261, 2012.

[17] E. Askari, F. Bobaru, R. Lehoucq, M. Parks, S. Silling, and O. Weckner, "Peridynamics for multiscale materials modeling," in *Journal of Physics: Conference Series*, vol. 125, p. 012078, IOP Publishing, 2008.

[18] B. Alali and R. Lipton, "Multiscale dynamics of heterogeneous media in the peridynamic formulation," *Journal of Elasticity*, vol. 106, no. 1, pp. 71–103, 2012.

[19] F. Bobaru, "Influence of van der Waals forces on increasing the strength and toughness in dynamic fracture of nanofibre networks: a peridynamic approach," *Modelling and Simulation in Materials Science and Engineering*, vol. 15, no. 5, p. 397, 2007.

[20] F. Bobaru and S. A. Silling, "Peridynamic 3D models of nanofiber networks and carbon nanotube-reinforced composites," in *MATERIALS PROCESSING AND DESIGN: Modeling, Simulation and Applications-NUMIFORM 2004-Proceedings of the 8th International Conference on Numerical Methods in Industrial Forming Processes*, vol. 712, pp. 1565–1570, AIP Publishing, 2004.

[21] F. Bobaru, S. Silling, and H. Jiang, "Peridynamic fracture and damage modeling of membranes and nanofiber networks," in *XI Int. Conf. Fract., Turin, Italy*, 2005.

[22] S. A. Silling and F. Bobaru, "Peridynamic modeling of membranes and fibers," *International Journal of Non-Linear Mechanics*, vol. 40, no. 2, pp. 395–409, 2005.

[23] A. Agwai, I. Guven, and E. Madenci, "Peridynamic theory for failure prediction in multilayer thin-film structures of electronic packages," in *58th Electronic Components and Technology Conference, IEEE 2008.*, pp. 1614–1619.

[24] A. Agwai, I. Guven, and E. Madenci, "Crack propagation in multilayer thin-film structures of electronic packages using the peridynamic theory," *Microelectronics Reliability*, vol. 51, no. 12, pp. 2298–2305, 2011.

[25] A. Agwai, I. Guven, and E. Madenci, "Damage prediction for electronic package drop test using finite element method and peridynamic theory," in *59th Electronic Components and Technology Conference, IEEE 2009.*, pp. 565–569.

[26] E. Celik, E. Oterkus, I. Guven, and E. Madenci, "Mechanical characterization of ultra-thin films by combining afm nanoindentation tests and peridynamic simulations," in *59th Electronic Components and Technology Conference, IEEE 2009.*, pp. 262–268.

[27] W. Lu and K. Komvopoulos, "Nanotribological and nanomechanical properties of ultrathin amorphous carbon films synthesized by radio frequency sputtering," *Journal of Tribology*, vol. 123, no. 3, pp. 641–650, 2001.

[28] S. A. Silling, M. Epton, O. Weckner, J. Xu, and E. Askari, "Peridynamic states and constitutive modeling," *Journal of Elasticity*, vol. 88, no. 2, pp. 151–184, 2007.

[29] R. B. Lehoucq and S. Silling, "Force flux and the peridynamic stress tensor," *Journal of the Mechanics and Physics of Solids*, vol. 56, no. 4, pp. 1566–1577, 2008.

[30] S. A. Silling and R. B. Lehoucq, "Convergence of peridynamics to classical elasticity theory," *Journal of Elasticity*, vol. 93, no. 1, pp. 13–37, 2008.

[31] M. L. Parks, P. Seleson, S. J. Plimpton, S. A. Silling, and R. B. Lehoucq, "Peridynamics with LAMMPS: A user guide v0.3 beta," Sandia Report 2011-8523, 2011.

[32] S. A. Silling and E. Askari, "A meshfree method based on the peridynamic model of solid mechanics," *Computers & Structures*, vol. 83, no. 17, pp. 1526–1535, 2005.

[33] L. Verlet, "Computer" experiments" on classical fluids. I. Thermodynamical properties of Lennard-Jones molecules," *Physical Reviews*, vol. 159, no. 1, p. 98, 1967.

[34] C. Casiraghi, J. Robertson, and A. C. Ferrari, "Diamond-like carbon for data and beer storage," *Materials Today*, vol. 10, no. 1, pp. 44–53, 2007.

[35] E. Madenci and E. Oterkus, *Peridynamic Theory and Its Applications*. Springer, 2014.

[36] F. Bobaru, M. Yang, L. F. Alves, S. A. Silling, E. Askari, and J. Xu, "Convergence, adaptive refinement, and scaling in 1D peridynamics," *International Journal for Numerical Methods in Engineering*, vol. 77, no. 6, pp. 852–877, 2009.

List of Tables

Table 1: Mechanical properties and critical stretch of silicon substrate and diamond tip

Material	Elastic modulus[(a)] (GPa)	Poisson's ratio[(a)]	Density[(a)] (g/cm^3)	Critical stretch
Silicon	132	0.278	2.329	0.01[(b)]
Diamond	1144	0.07	3.515	0.035

[(a)] Ref. [27]
[(b)] Ref. [24]

Table 2: Thickness, rms roughness, elastic properties, density, and critical stretch of a-C films used in peridynamic friction analysis [27].

Film #	Thickness (nm)	rms (nm)	Elastic modulus (GPa)	Poisson's ratio	Density (g/cm^3)	Critical stretch
1	31	0.51	105	0.278	3.139	0.0125
2	34	0.20	197	0.278	4.058	0.0125
3	39	0.15	206	0.278	4.143	0.0125
4	53	0.27	139	0.278	3.500	0.0125
5	59	0.23	101	0.278	3.094	0.0125
6	69	0.15	192	0.278	4.017	0.0125
7	95	0.24	155	0.278	3.661	0.0125

Table 3: Thickness, rms roughness, elastic properties, density, and critical stretch of a-C films used in peridynamic wear analysis [27].

Film #	Thickness (nm)	rms roughness (nm)	Elastic modulus (GPa)	Poisson's ratio	Density (g/cm^3)	Critical stretch
8	17	0.19	113	0.278	3.230	0.0125
9	22	0.18	203	0.278	4.115	0.0125
10	10	0.2	226	0.278	4.317	0.0125

Table 4: Coefficient of friction results of m-convergence tests.

δ(nm)	m	Coefficient of friction
8	3.5	0.1441
8	4	0.1534
8	4.5	0.1588
8	5	0.1412

Table 5: Comparison of analytical and experimental results of the coefficient of friction of a-C films versus film thickness, rms roughness, and normal load.

Film #	Thickness[(a)] (nm)	rms roughness[(a)] (nm)	Normal load	Coefficient of friction	
				Peridynamics	Experimental[(a)]
1	31	0.51	50	0.148	0.16
			100	0.131	0.14
			200	0.119	0.13
			400	0.105	0.12
2	34	0.20	50	0.157	0.17
			100	0.134	0.15
			200	0.116	0.14
			400	0.106	0.12
3	39	0.15	50	0.165	0.18
			100	0.145	0.16
			200	0.128	0.14
			400	0.119	0.13
4	53	0.27	50	0.158	0.17
			100	0.139	0.15
			200	0.122	0.13
			400	0.108	0.12
5	59	0.23	50	0.153	0.17
			100	0.134	0.15
			200	0.108	0.14
			400	0.107	0.12
6	69	0.15	50	0.177	0.18
			100	0.155	0.16
			200	0.136	0.14
			400	0.124	0.13
7	95	0.24	50	0.154	0.17
			100	0.133	0.15
			200	0.125	0.13
			400	0.114	0.12

[(a)] Ref. [27]

Table 6: Comparison of analytical and experimental results of the wear depth of a-C films versus film thickness, rms roughness, and normal load

Film #	Wear depth (nm)	
	Peridynamics	Experimental[(a)]
8	0.710	0.76
9	0.382	0.40
10	0.134	0.20

[(a)] Ref. [27]

List of Figures

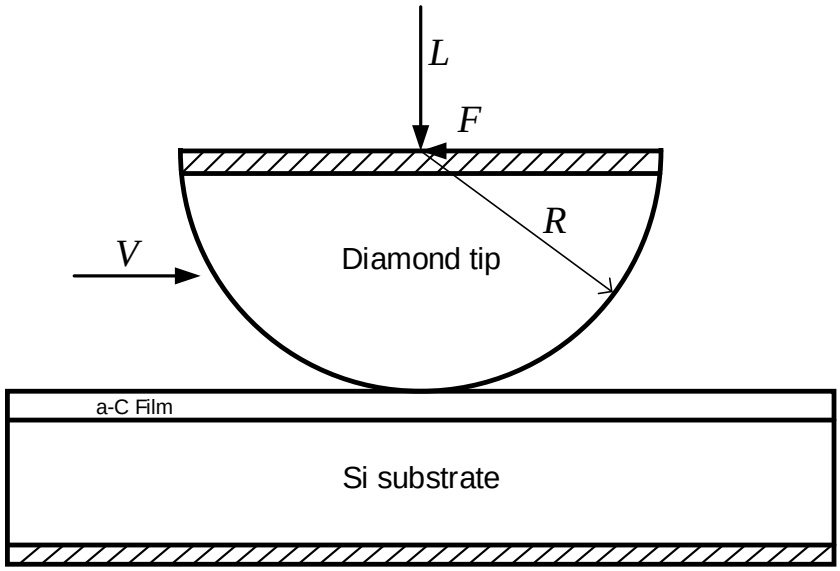

Figure 1: Schematic of peridynamics friction model of a spherical diamond tip sliding against an a-C thin film strongly adhered to a Si substrate. The shaded thin layer at the bottom of the substrate and the top of the tip is modeled as rigid. The coefficient of friction is obtained as the ratio of the tangential (friction) force F and the applied normal load L

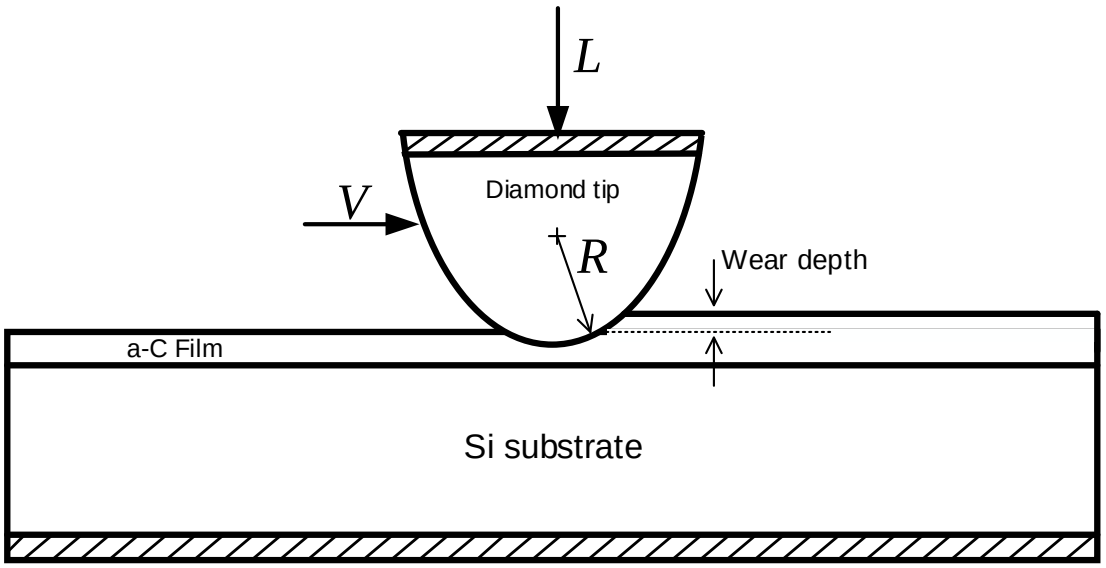

Figure 2: Schematic of peridynamics wear model of a sharp spherical diamond tip under a normal load L plowing through an a-C thin film strongly adhered to a Si substrate. The shaded thin layer at the bottom of the substrate and the top of the tip is modeled as rigid.

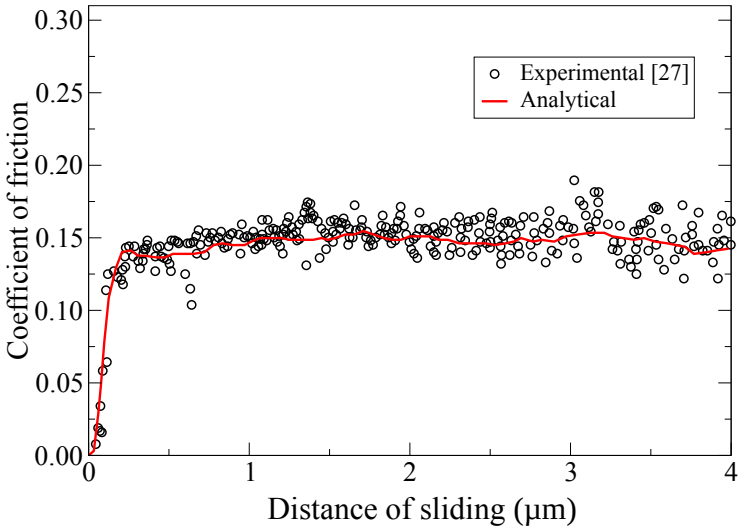

Figure 3: Analytical and experimental results of the coefficient of friction of a-C films versus sliding distance for a normal load equal to 400 μN.

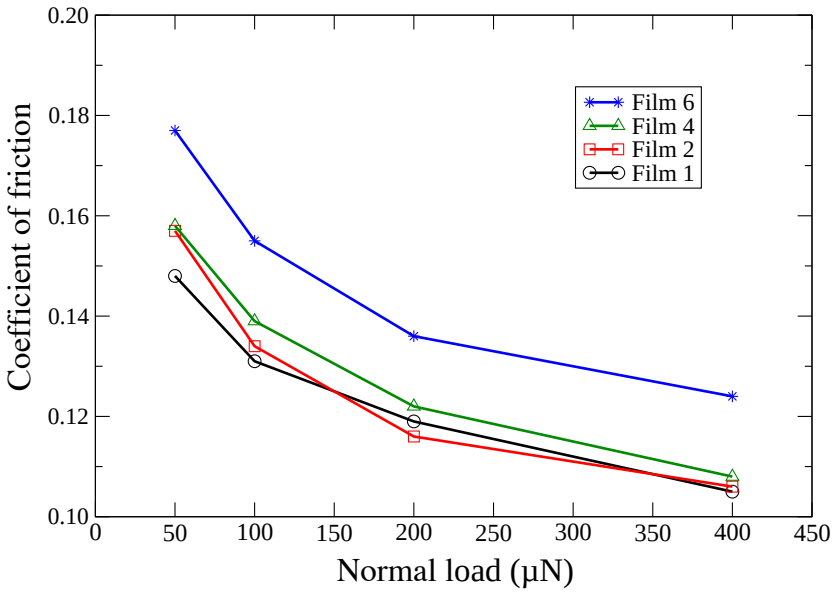

Figure 4: Analytical results of the coefficient of friction of a-C films versus normal load.